

UCLA

UCLA Previously Published Works

Title

Determining PTEN functional status by network component deduced transcription factor activities.

Permalink

<https://escholarship.org/uc/item/4h4863b7>

Journal

PloS one, 7(2)

ISSN

1932-6203

Authors

Tran, Linh M
Chang, Chun-Ju
Plaisier, Seema
et al.

Publication Date

2012

DOI

10.1371/journal.pone.0031053

Peer reviewed

Determining PTEN Functional Status by Network Component Deduced Transcription Factor Activities

Linh M. Tran^{1,2,3}, Chun-Ju Chang^{1,3,4}, Seema Plaisier¹, Shumin Wu^{1,2}, Julie Dang⁴, Paul S. Mischel^{2,4,6}, James C. Liao⁵, Thomas G. Graeber^{1,2,3}, Hong Wu^{1,6*}

1 Department of Molecular and Medical Pharmacology, University of California Los Angeles, Los Angeles, California, United States of America, **2** Institute for Molecular Medicine, University of California Los Angeles, Los Angeles, California, United States of America, **3** Crump Institute for Molecular Imaging, University of California Los Angeles, Los Angeles, California, United States of America, **4** Department of Pathology and Laboratory Medicine, University of California Los Angeles, Los Angeles, California, United States of America, **5** Department of Chemical and Biomolecular Engineering, University of California Los Angeles, Los Angeles, California, United States of America, **6** Eli and Edythe Broad Center of Regenerative Medicine and Stem Cell Research, University of California Los Angeles, Los Angeles, California, United States of America

Abstract

PTEN-controlled PI3K-AKT-mTOR pathway represents one of the most deregulated signaling pathways in human cancers. With many small molecule inhibitors that target PI3K-AKT-mTOR pathway being exploited clinically, sensitive and reliable ways of stratifying patients according to their PTEN functional status and determining treatment outcomes are urgently needed. Heterogeneous loss of PTEN is commonly associated with human cancers and yet PTEN can also be regulated on epigenetic, transcriptional or post-translational levels, which makes the use of simple protein or gene expression-based analyses in determining PTEN status less accurate. In this study, we used network component analysis to identify 20 transcription factors (TFs) whose activities deduced from their target gene expressions were immediately altered upon the re-expression of PTEN in a PTEN-inducible system. Interestingly, PTEN controls the activities (TFA) rather than the expression levels of majority of these TFs and these PTEN-controlled TFAs are substantially altered in prostate cancer mouse models. Importantly, the activities of these TFs can be used to predict PTEN status in human prostate, breast and brain tumor samples with enhanced reliability when compared to straightforward IHC-based or expression-based analysis. Furthermore, our analysis indicates that unique sets of PTEN-controlled TFAs significantly contribute to specific tumor types. Together, our findings reveal that TFAs may be used as “signatures” for predicting PTEN functional status and elucidate the transcriptional architectures underlying human cancers caused by PTEN loss.

Citation: Tran LM, Chang C-J, Plaisier S, Wu S, Dang J, et al. (2012) Determining PTEN Functional Status by Network Component Deduced Transcription Factor Activities. PLoS ONE 7(2): e31053. doi:10.1371/journal.pone.0031053

Editor: Dean G. Tang, The University of Texas M.D. Anderson Cancer Center, United States of America

Received: September 9, 2011; **Accepted:** January 1, 2012; **Published:** February 8, 2012

Copyright: © 2012 Tran et al. This is an open-access article distributed under the terms of the Creative Commons Attribution License, which permits unrestricted use, distribution, and reproduction in any medium, provided the original author and source are credited.

Funding: LMT is supported by NIH T32 CA009056. This work has been supported in part by award from the Prostate Cancer Foundation and grant from NIH (R01 CA107166, R01 CA121110 and P50 CA092131 to HW). The funders had no role in study design, data collection and analysis, decision to publish, or preparation of the manuscript. No additional external funding received for this study.

Competing Interests: The authors have declared that no competing interests exist.

* E-mail: hwwu@mednet.ucla.edu

These authors contributed equally to this work.

Current address: Department of Molecular and Cellular Oncology, The University of Texas MD Anderson Cancer Center, Houston, Texas, United States of America

Introduction

The *PTEN* (phosphatase and tensin homologue deleted on chromosome 10) tumor suppressor gene is mutated frequently in human cancers and cancer predisposition disorders [1,2]. PTEN status not only plays a role in tumorigenesis, but also a crucial determinant for efficacy of cancer treatments. It has been shown that tumors with PTEN deficiency do not respond to Her2 inhibitor [3] or EGFR inhibitor [4] treatments whereas restored PTEN activity sensitized the tumor cells to these treatments. Accumulated evidence suggest that PTEN functional deficiency can result from different mechanisms, including *PTEN* genomic deletion, gene mutations, epigenetic silencing (e.g. silencing by DNA methylation or miRNAs), impaired membrane recruitment (e.g. loss of interaction with MAGI2) or decreased protein stability/activity mediated by various post-translational modification (e.g. phosphorylation, acetylation, oxidation, ubiquitination) [5,6]. Therefore, it is rather difficult to determine PTEN

functional status using simple gene expression or immunohistochemistry analysis.

Determination of PTEN functional status can be further complicated by the intricate signaling pathways that are regulated by PTEN. Through its lipid phosphatase activity, PTEN regulates PI3K-AKT-mTOR signaling that are involved in downstream transcription machineries, such as NF- κ B, FOXO, and p53 [7,8,9,10,11]. PI3K-AKT signaling also engages other associated signaling networks and key factors responsible for cell size, cell motility, cell cycle, and cell death regulation [12]. Although regulation of PTEN-PI3K-AKT signaling cascade has been vigorously exploited, the multi-level controls of PTEN expression and activity and the complexity of feedback regulatory loops from PI3K downstream effectors to upstream receptor tyrosine kinase expression and activities have made determination of PTEN functional status and response of PTEN deficient tumors towards PI3K-AKT-mTOR pathway inhibition difficult. For example, inhibitors targeting PI3K, AKT and mTOR have been tested in

multiple clinical trials [13]; however, it is recently reported that AKT inhibitors can induce the expression and phosphorylation of multiple upstream receptor tyrosine kinases (RTKs) whereas mTOR inhibitor rapamycin can activate AKT through a negative feedback mechanism [14]. Thus, the phospho-status of individual downstream signaling components, such as P-AKT and P-S6K, may not accurately represent PTEN status nor reflect the ultimate activation status of the PI3K/AKT signaling pathway.

To decipher functional status of PTEN and PTEN-controlled signaling network, we first analyzed the transcriptional targets which are immediately regulated by *PTEN* expression using global gene expression profiling in a *PTEN* inducible system. We further hypothesized that vast target gene expression changes may be controlled by a few key transcription factors (TFs), which can be a more sensitive and accurate “signature” for PTEN status. However, expression levels of these TFs will not always be sufficient to reflect their activity since the activity of a transcription factor (TFA) is controlled by various post-translational modifications as well as co-activator and co-repressor activities. Previous works by us and others have shown that TFA can be best inferred from the transcript levels of its direct target genes, rather than its mRNA level using Network Component Analysis (NCA) [15,16,17]. NCA is a model-based decomposition method to deduce transcription factor activity (TFA) and regulation control strength (CS) of TFs from target gene expression and information of TF - gene interactions. The information of TF - gene interaction, or network connectivity, is constructed by chromatin immunoprecipitation (ChIP) analysis [18], DamID methylation profiling [19] or extensive literature search [20].

In this study, we identified 20 TFs whose activities are immediately altered upon the reexpression of *PTEN* (see Figure 1A for our overall strategy) in the *Pten* null mouse embryonic fibroblasts (MEFs). We found that the activities of these PTEN-controlled TFs are significantly altered in prostate cancer mouse models. Furthermore, the TFAs of these TFs show enhanced sensitivity and specificity when used to predict PTEN status in human prostate, breast and brain tumors, as compared to the gene expression-based analysis.

Results

Identification of transcription factors whose activities are perturbed by PTEN re-expression

To identify transcription factors whose expressions or activities are directly regulated by *PTEN* re-expression, an inducible system was generated in which *PTEN* expression can be controlled in a doxycycline-dependent manner in the *Pten* null *Pten^{ΔloxP}/ΔloxP* cells [21]. PTEN protein level was significantly induced one day after 20 μg/ml doxycycline treatment and approached WT level on day 2 (Figure 1B; *Pten^{L/L}* is a *Pten* WT line and isogenic to *Pten^{ΔloxP}/ΔloxP*). Consistent to our previous study, re-expression of *PTEN* was able to suppress the gene expression of p90^{MDM2} isoform without significant change in p76^{MDM2} isoform as previously reported (Figure S1A) [21].

Next we analyzed global gene expression alterations immediate following *PTEN* re-expression by comparing gene expression levels 1 and 2 days after doxycycline (20 μg/mL) treatment with those before the treatment (Figure 1C; 1-0 and 2-0) and identified 352 genes whose expressions are changed by 2-fold within 2 days upon *PTEN* re-expression. Among these PTEN-induced genes, 136 (38.6%) are up regulated and 216 (61.4%) are down regulated by *PTEN* re-expression. Table S1 lists these genes along with their fold changes after inducing PTEN expression.

We reasoned that the PTEN-inducible genes must be regulated by the key transcription factors whose activities are controlled by PTEN. Therefore, we investigated PTEN immediately controlled TFs via network component analysis (NCA) in which the activities of TFs (TFAs) are deduced based on expression of their target genes. Different from conventional gene expression analysis, which focuses on statistically significant changes of individual genes, NCA deduces TFAs based on the concordant variations of all, rather than individual target genes, and that does not require the analyzed gene expressions to be statistically significant [15]. We recently developed a new NCA complementary algorithm [16] that allows analysis of mammalian datasets with limited number of data points for re-constructing a complicated network with multiple TFs. Specifically, this trimming algorithm removes the false positive interactions between TFs and their target genes, detected via high throughput ChIP-chip analysis, and enables the key target genes of the TFs of interest to be revealed [16].

We used NCA and the trimming algorithm to construct the transcription network, based on 70 known TFs and their controlled 782 target genes [20]. Heatmaps in Figure 1C shows that 20/70 TFs whose activities (TFAs) are immediately altered by *PTEN* re-expression (Figure 1C, right; $p < 0.05$, 2-tail z-test). Interestingly, only *Egr1* and *c-Jun* show >2-fold changes in their gene expression levels [22] and NF-κB, *c-Myc*, *Relb*, *Smad1/7* show 1.5–2.0-fold of changes. These data imply that *PTEN* expression may influence the activities of these transcription factors without significantly changing their expression levels. Of note, several TFs, such as NF-κB and Hif1α, have been described as PTEN pathway-regulated TFs by previous reports [23,24]. Unfortunately, *Foxo*, which is also known to be regulated by PTEN controlled AKT activity, is not included in this analysis since its target gene expression values are not available. We refer these 20 TFs as PTEN-controlled TFs whose activities depend on PTEN expression status.

PTEN re-expression down-regulates transcription activities of c-MYC and LEF1

To validate the PTEN-controlled TFs identified in *PTEN* inducible MEF cells, we employed another *PTEN*-inducible system, the *PTEN* null human prostate cancer cell line PC3 [6,25]. By using human cell line, we are able to link PTEN-controlled TFs in mouse model to human cancers. Similar to our observation in the inducible-*Pten^{ΔloxP}/ΔloxP* MEFs, PTEN protein expression is significantly induced after 1 and 2 days of doxycycline treatment in the inducible-PTEN PC3 cells (Figure 2A). Using qPCR analysis, we found that the expression levels of *c-MYC* and *LEF1* after PTEN re-expression in PC3 cells also echoed those from the MEF-derived data: *c-MYC* gene expression is down-regulated ($p < 0.05$) while *LEF1* expression level remained constant (Figure 1C and 2B). We also measured the total protein level of c-MYC and phosphorylated to total protein ratios of STAT6 and c-JUN and found no substantial changes in c-MYC and STAT6 after PTEN re-expression (Figure S1B). In contrast, the ratio of phospho-c-JUN to total c-JUN is reduced by more than 2-fold after *PTEN* re-expression, consistent with our previous study [26].

The MEF system results predict that transcription activity of c-MYC would be down regulated by *PTEN* re-expression in the PC3 system. To validate this, we examined the association between c-MYC and the promoters of its target genes using chromatin immunoprecipitation (ChIP) analysis. c-MYC target genes *BCAT1*, *CDK4*, *EIF4E*, and *SHMNT1* were selected because (1) their proximal promoter regions contain c-MYC consensus binding sequence (CACGTG), which is conserved between human and

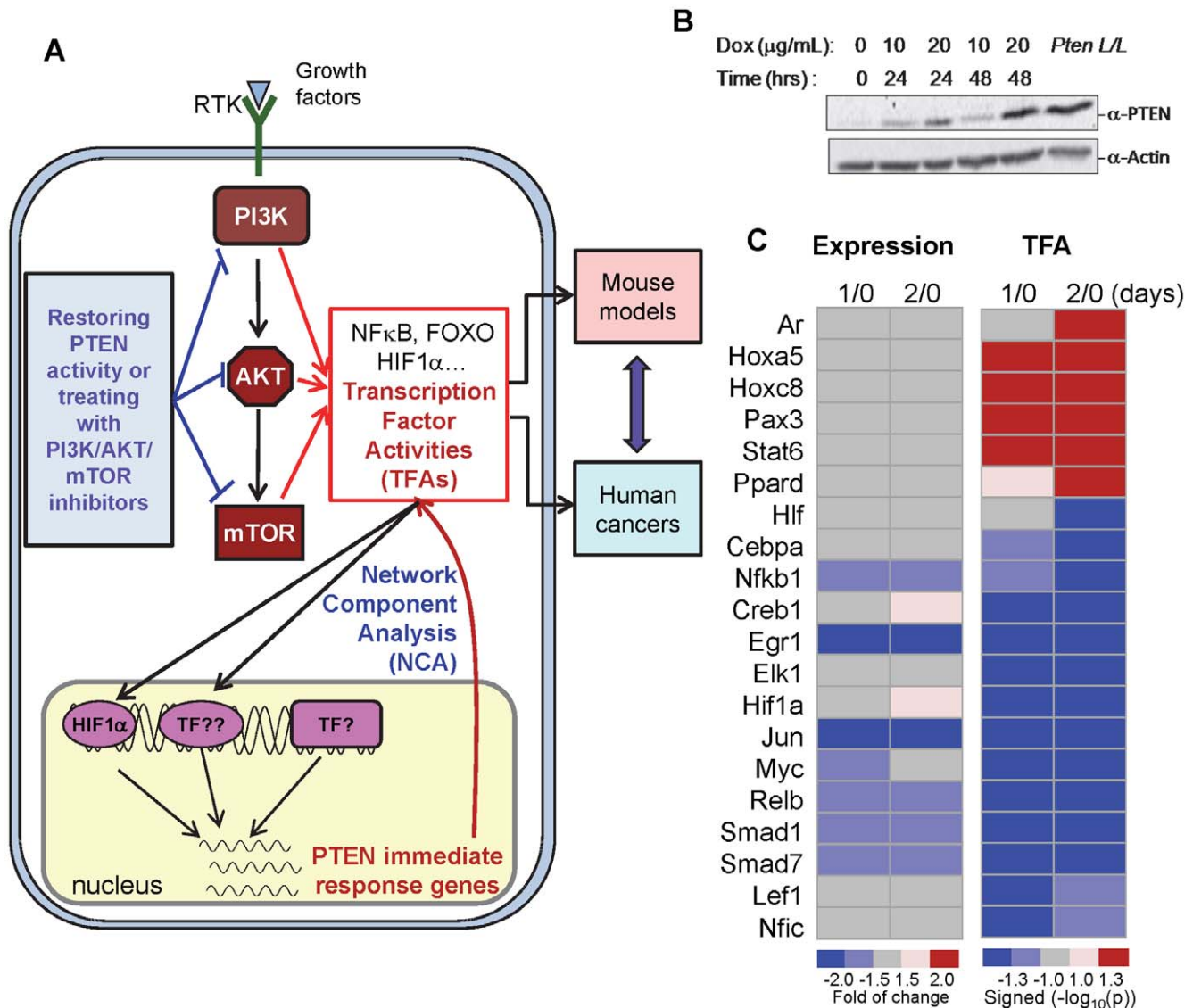


Figure 1. PTEN re-expression regulates transcription factor expression and activity in PTEN-inducible *Pten*^{flox/flox} MEFs. (A) Schematic illustration of rationale and approach used in this study. To identify PTEN-controlled TFs, their activities (TFAs) in PTEN inducible system were first derived from expression of their target genes by NCA. The perturbed TFs were then examined further in mouse models and human cancers. (B) Immunoblot showing PTEN expression levels at 0, 1, and 2 days after treatment with the indicated concentration of Doxycycline in *Pten*^{flox/flox} MEFs. Isogenic WT cells (*Pten*^{L/L}) were used as a positive control. (C) Heatmaps showing the changes of expression and activity (TFA) of transcription factors in fold and log₁₀ transformed p-value of the z-test, respectively, caused by PTEN re-expression for 1 day (1/0) or 2 days (2/0). doi:10.1371/journal.pone.0031053.g001

mouse; and (2) the control strengths by c-MYC were highly significant based on NCA analysis (Figure 1C). We found that *PTEN* re-expression significantly decreases the association of c-MYC to the promoter of its target genes (Figure 2C top panel), and that in turn reduces expressions of these c-MYC target genes (Figure 2C bottom bar graph). Since *PTEN* re-expression does not change the total c-MYC protein level, *PTEN* must modulate c-MYC transcription factor activity by either regulating the half-life of c-MYC or the activities of its binding partners. Similarly, *PTEN* re-expression also decreases the association of LEF1 to the promoter of its target gene *WISP1*, and that leads to concurrent reduction of its gene expression (Figure 2D). These results suggest that transcription activities of both c-MYC and LEF1 are perturbed by *PTEN* expression. Furthermore, our data show that in addition to transcriptional activity, *PTEN* induction also reduces

c-MYC gene expression, suggesting *PTEN*-mediated suppression of c-MYC activity might be partially contributed by its decreased expression. However, *PTEN* appears to impact solely on LEF1 activity without altering mRNA expression of the transcription factor itself.

The activities of PTEN-controlled TFs are substantially altered in murine prostate cancer models *in vivo*

PTEN plays a critical role in human and murine prostate tumorigenesis [1,27,28]. To determine whether TFAs deduced from *PTEN*-inducible MEF reflect *PTEN* functional status *in vivo*, we examined the TFAs, based on the gene expression datasets we have in hand, of three well-established murine prostate cancer models, i.e. the *Pten* null [29], the *MAK1* [24], and the *hi-c-Myc* [30] models (Figure 3A), and then categorized the TFs into

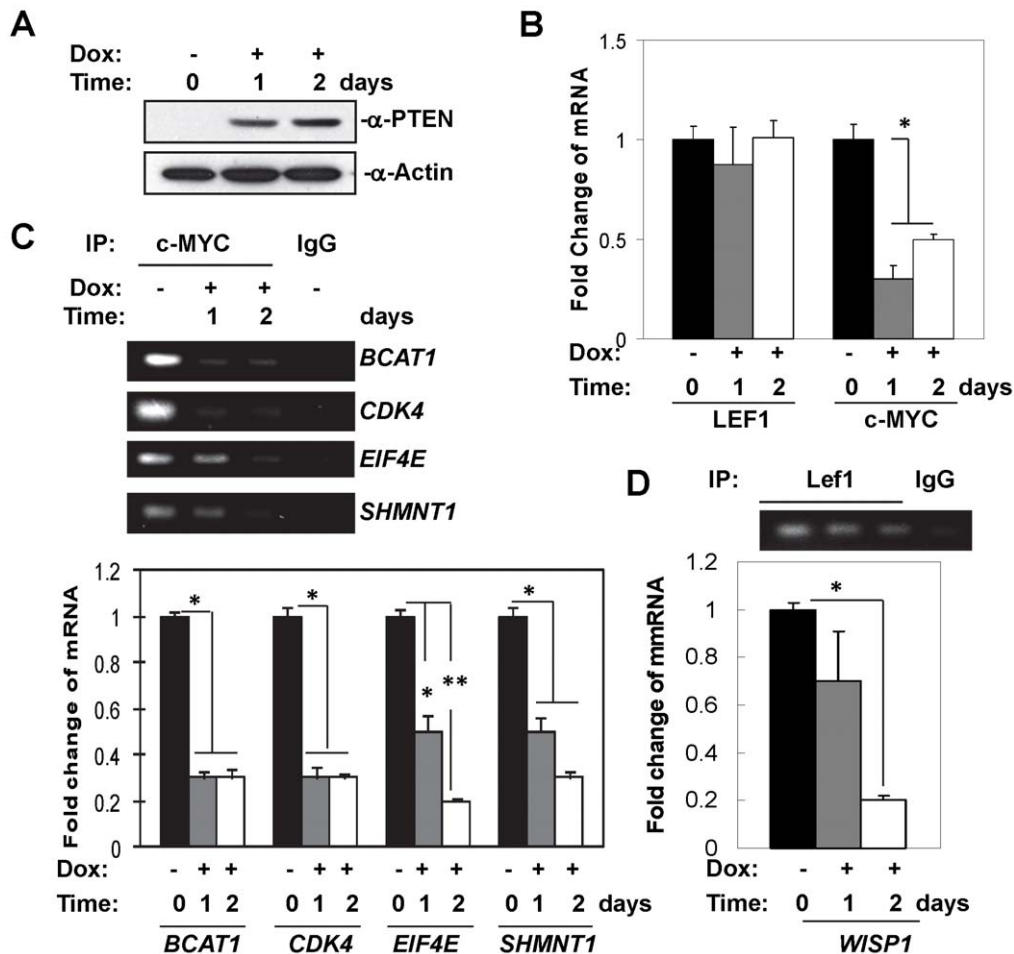


Figure 2. PTEN re-expression downregulates activities of c-MYC and LEF1 in PTEN-inducible PC3 cells. (A) Immunoblot showing PTEN expression levels under Doxycycline induction. (B) Bar graphs showing fold changes of c-MYC and LEF1 mRNA expression by qPCR analysis. (C and D) Bar graphs showing the target gene expression of c-MYC and LEF1 by qPCR analysis, respectively. * $p < 0.05$ and ** $p < 0.01$. doi:10.1371/journal.pone.0031053.g002

subgroups according to alterations of their activities in these mouse models (Figure 3B). Figure S2 illustrates the TFA profiles in all three murine models. As expected, the total numbers of perturbed TFs in murine cancer models is higher than that in PTEN inducible system. Among the 20 PTEN-controlled TFs identified in the *Pten* MEF system, all except Hlf are significantly altered in at least one of the models. *Egr1* has its activity altered solely in the *Pten* null murine model. Eight TFs (marked in bold in Figure 3A) exhibit concordant alterations when the PTEN downstream AKT/mTOR pathway is manipulated genetically or pharmacologically (Rapamycin treated *mAKT1* model). Interestingly, *hi-c-Myc* shares 13 TFAs changes with *Pten* null or *Pten* null and *mAKT1* models, of which seven are concordantly regulated, including *Ar*, *Creb1*, *Hoxc8*, *Elk1*, *Smad1*, *Hif1 α* , *Stat6* and *c-Myc* (Figure 3B). Since *c-Myc* transcription level and activity is regulated by PTEN, these seven TFAs may reflect the epistatic component of PTEN/AKT/mTOR and *c-Myc*. The remaining 5 TFAs (* in Figure 3A and B) are discordantly regulated by *c-Myc* and the PTEN/AKT/mTOR pathway, either due to non-overlapping function and/or additional alterations accumulated in vivo during tumor initiation and progression of these in vivo models. In brief, the activities of the majority of PTEN-controlled TFs are altered in the murine prostate cancer models in vivo, and the variations among the models might be explained by different genetic background and stage of tumor development.

Signature of PTEN-controlled TFs correlates with PTEN status in human cancers

We hypothesized that the TFAs controlled by PTEN expression should reflect PTEN functional status in human cancers. To test the hypothesis, we examined if tumor subgroups determined by TFA-based unsupervised clustering are enriched for tumors with distinct PTEN status. For this, we focused on prostate, breast and brain tumors because 1) PTEN deficiency frequently occurs in these cancers [27,31,32], and 2) large gene expression datasets are publically available [32,33,34]. Out of 19 PTEN-controlled TFs (AR is removed from our analysis to prevent bias toward prostate), we were able to derive 16, 15 and 16 TFAs from human prostate, breast and brain tumor datasets, respectively, based on the availability of their target gene expression values in the datasets. For each cancer type, patient samples were first classified by unsupervised clustering based on the signature TFAs then annotated with their associated pathological grades or PTEN status, determined by either CGH analysis for PTEN copy number (CN) alterations in prostate cancers [35] or immunohistochemistry (IHC) and mRNA array for PTEN expression in breast cancers [32]. For brain tumors, PTEN status was first predicted by TFAs-based unsupervised clustering, and then confirmed by us in a majority of the samples by IHC analysis.

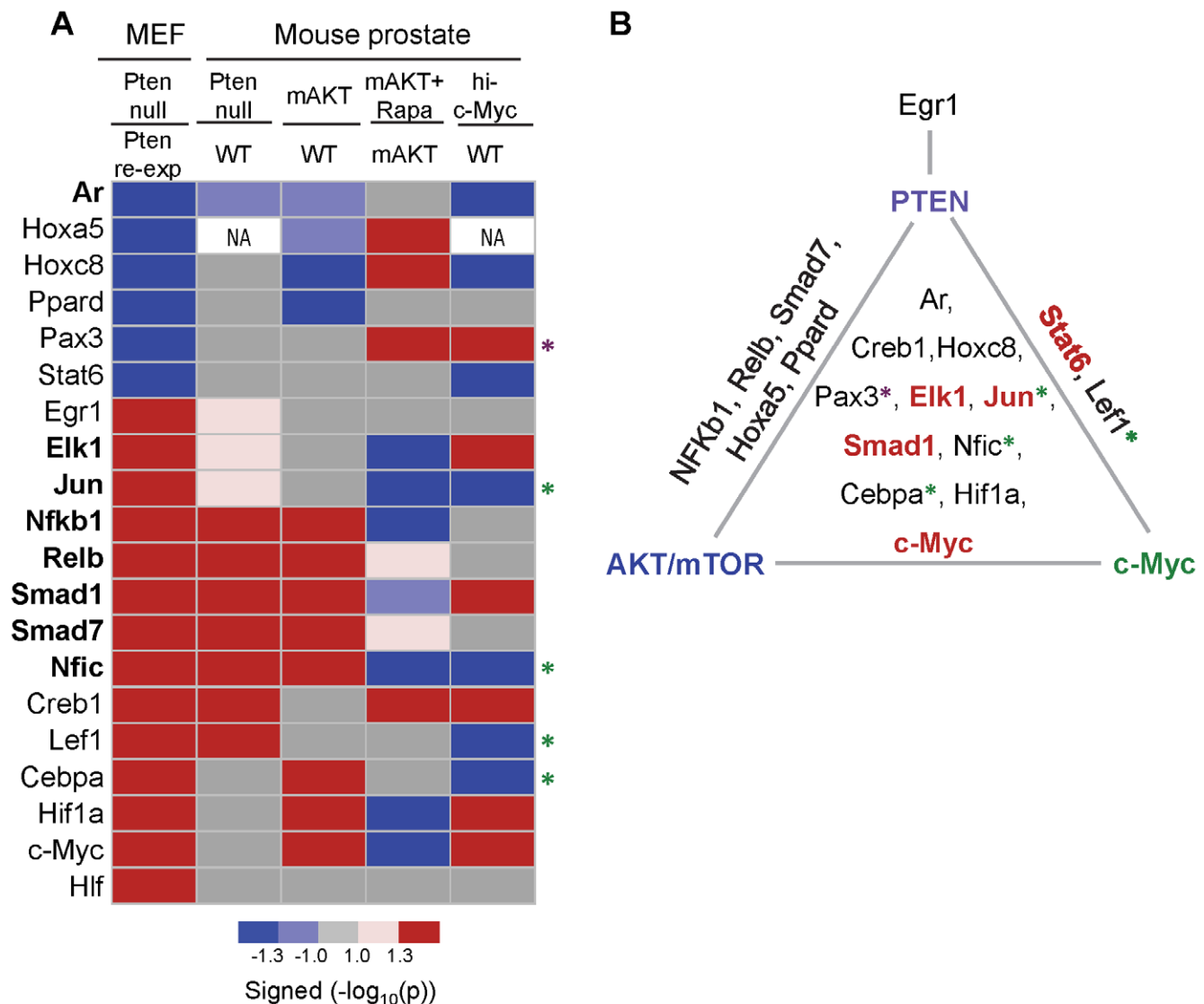


Figure 3. PTEN-regulated TFs are significantly increased in murine prostate cancer models *in vivo*. (A) Heatmap showing changes of PTEN-regulated TFs in PTEN inducible MEFs (PTEN null compared to PTEN re-expression or PTEN WT) and murine prostate cancer models (compared to WT control mice; Rapa: Rapamycin treatment). TFs regulated by PTEN/AKT/mTOR pathway are marked in bold. TFs exhibit discordant regulation between c-Myc and the PTEN/AKT/mTOR pathway are marked by *. The purple and green asterisks indicate Myc-activating and suppressing TFs respectively. (B) Triangle diagram summarizing the TFs regulated by PTEN, AKT/mTOR and/or c-MYC.
doi:10.1371/journal.pone.0031053.g003

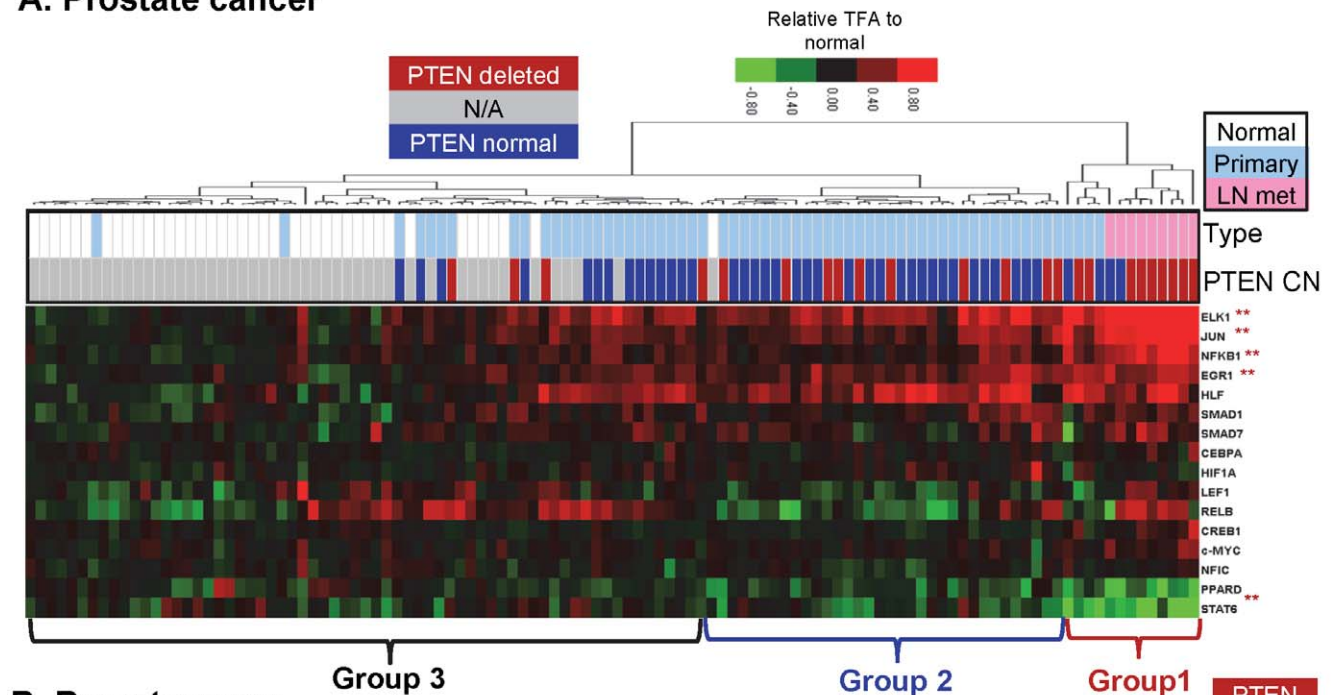
As shown in Figure 4A, PTEN-controlled TFs separate 112 prostate samples into three distinct groups. Group 1 contains mostly lymph node metastatic samples in which 69% (9/13) have deleted PTEN based on CN; Group 2 has mostly primary cancer samples in which 31% (11/35) have PTEN CN changes, whereas Group 3 consists of a majority of normal prostate cancer samples with only 4.7% (3/64) PTEN CN changes. Of note, the overall rates of PTEN CN alterations found in this cohort fit well with the results from integrated genomic profiling of a larger group of human prostate cancer samples [27]. The heatmap of clustered TFA levels shows that the activities of EGR1, ELK1, JUN, and NF- κ B1 are significantly (*, t-test $p < 0.001$) higher in PTEN negative samples while STAT6 activity is lower in PTEN negative samples, as compared to those in the PTEN positive samples (Figure 4A).

PTEN-controlled TFA patterns can also be used as signatures to separate PTEN negative from PTEN positive breast cancers (Group 1 vs. Group 3 respectively in Figure 4B and S3A). The

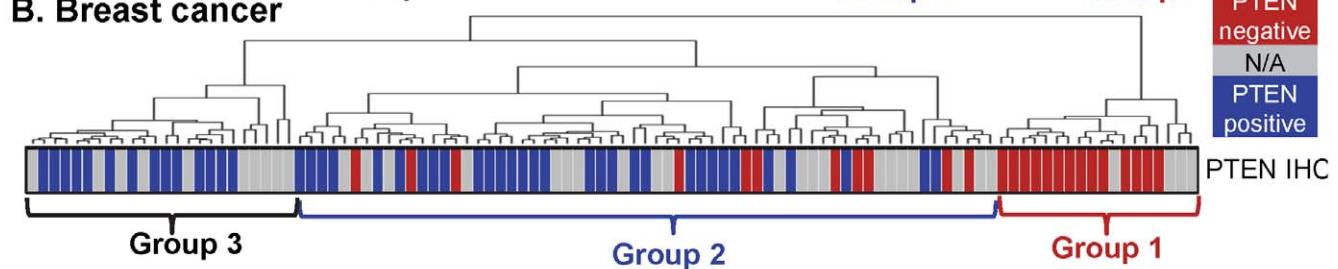
same TFA-based analysis on Netherland Cancer Institute (NKI) published breast cancer dataset that does not have associated PTEN status [36], also classifies breast cancer in three subgroups, and the Group 1, predicted to be PTEN negative, is associated with poor differentiated, ER-negative basal-like phenotype [37] (Figure S3B), which is consistent with our recent publication [38].

Similarly, PTEN-controlled TFs can separate grade 4 glioblastomas from grade 3 gliomas (Group 1 vs. Group 2 in Figure 4C and S3C). As expected, patients within the PTEN TFA-positive group (Group 2) have mostly grade 3 tumors and longer disease specific survival (DSS) while patients within the PTEN TFA-negative group (Group 1) have more aggressive tumors and shorter DSS. We then compared DSS of patients within Group 1 whose PTEN status were determined by IHC analysis (PTEN IHC positive = blue bar, 17 patients; PTEN IHC negative = red bar, 16 patients) and found that PTEN IHC-positive patients have nearly identical DSS as PTEN IHC-negative patients (log-rank test

A. Prostate cancer



B. Breast cancer



C. Brain cancer

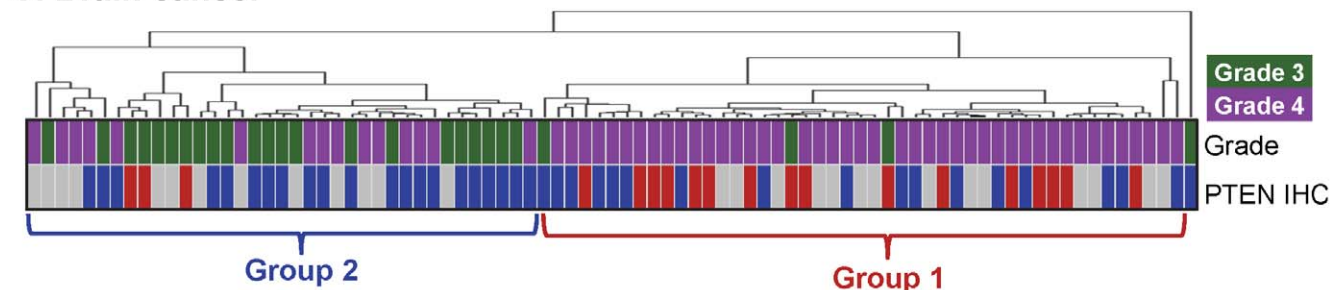


Figure 4. PTEN-controlled TFs predict PTEN status in human cancers. Unsupervised clustering analysis, based on PTEN-controlled TFAs, was used to classify human tumor samples. (A) In prostate cancer, group 1 is largely composed by samples with PTEN copy number changes (CN, red) and lymph node metastases (LN met, pink); Group 2 are primary cancer samples (light blue) with normal PTEN karyotype (blue) that are separated from most of normal prostate tissues (white). TFAs that are significantly altered between group 1 and group 3 are marked by **, $p < 0.001$. The heatmap was plotted based on relative changes to the respective average TFAs of normal samples. (B) In breast cancer, group 1 is mostly comprised of samples with PTEN-negative status (red) identified by immunohistochemistry (IHC). The majority of the samples in group 3 have positive PTEN status (blue), while group 2 includes both positive and negative PTEN samples. (C) In brain tumors, most samples in group 1 are associated with PTEN negative status (red). The PTEN negative subgroup is also correlated with higher tumor grade (green for grade 3 and purple for 4, respectively). doi:10.1371/journal.pone.0031053.g004

$p = 0.8$, Figure 5A). Thus, PTEN IHC status does not significantly segregate patients in terms of the functional outcome of DSS, while PTEN TFA status does. This analysis illustrates the advantage of using TFA-based signatures in evaluating PTEN functional status over traditional IHC-based analysis. Together, these results reveal the power of our approach in predicting PTEN status and its pathological association in human cancers in general.

Predicting PTEN status using murine and human cancer deduced TFA signatures

In addition to the PTEN-controlled TFAs derived from the inducible *Pten*^{ΔloxP/ΔloxP} MEFs, we identified another 19 TFs whose activities are significantly perturbed in the *Pten* null prostate cancer mouse model (Figure S2). These TFAs are not changed by transient *PTEN* re-expression in the MEF cell line. Interestingly,

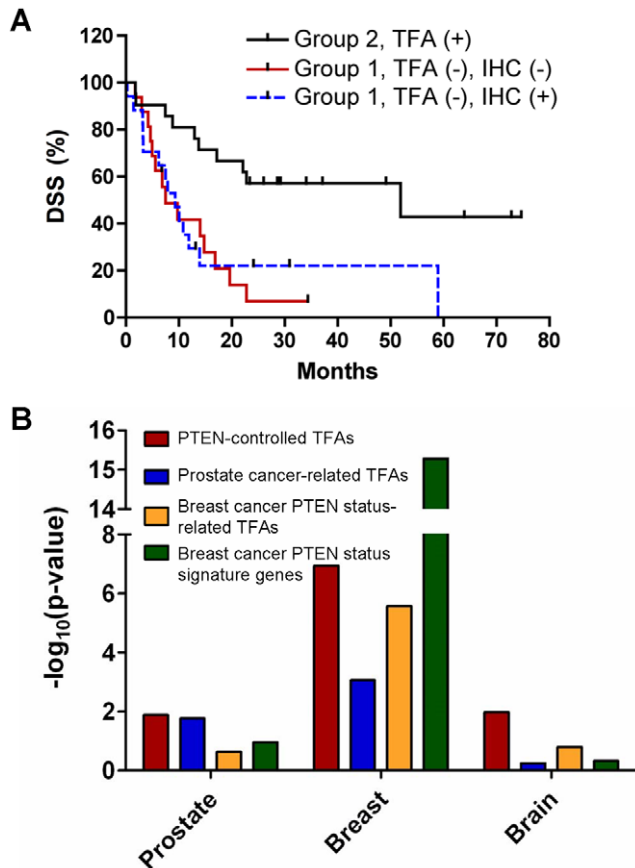


Figure 5. Enhanced robustness of TFA-based signatures in predicting PTEN status in human cancer. (A) The Kaplan-Meier survival curves of patients with brain tumors stratified according to PTEN-controlled TFA and IHC analyses. (B) \log_{10} transformed p-values of the χ^2 test evaluating the association of PTEN status with the hierarchical clustering-determined groups of human tumors. Clustering results are based on PTEN-controlled TFAs (red; Figure 3), prostate cancer-related TFAs (blue), TFA-based (gold) and gene expression-based (green) signatures derived from PTEN IHC data in breast tumors. When three major clusters are observed in prostate and breast cancers, the χ^2 tests are performed to associate different PTEN status in group 1 and groups 2 plus 3.
 doi:10.1371/journal.pone.0031053.g005

16 out of these 19 TFAs are concordantly regulated in the *mAKT1* and *hi-c-Myc* models and are also altered upon rapamycin treatment of the *mAKT1* model. Since these TFAs are not subject to the control of PTEN re-expression and may reflect the common pathological changes associated with these prostate cancer models, we coined them “prostate cancer-related TFAs”. We tested the power of both the PTEN-controlled TFAs that were defined in the Pten inducible MEF system, and the prostate cancer-related TFAs in predicting PTEN status in human cancers. The prostate cancer-related TFA signatures can be used to classify PTEN status in human prostate cancers to a similar accuracy as the PTEN-controlled TFAs, but they had less cross-tissue predictive power as they failed to reach significance levels when applied to breast and brain tumors (Figure 5B, blue bars).

Gene expression signatures, extracted from dysregulated genes in PTEN deficient cancer samples, have been used to predict PTEN status in human breast cancers [32]. We therefore, compared gene expression signature-based predictions to inferred TFA signature-based predictions of PTEN status in human cancer

samples. Applying our trimming NCA algorithm to the breast data set annotated with PTEN IHC status, we identified 15 TFs whose inferred TFAs were significantly altered (t-test $p < 0.0001$) (Figure S4). Among these six, HLF, JUN, c-MYC, EGR1, SMAD1, and HIF1A, were also identified as PTEN-controlled TFs (Figure 1C), and four, ESR2, MYB, RELA, and USF1, as prostate cancer-related TFs (Figure S2). 246 signature genes predictive of PTEN status had been previously reported in the breast cancer dataset [32]. Among these, 103 and 123 genes, respectively, had their expression values measured in the prostate and brain cancer datasets. As shown in Figure 5B, although both gene expression-based (green bars) and TFA-based (gold bars) breast PTEN IHC-based signatures can be used to predict PTEN status by unsupervised clustering approach in human breast cancers, they failed to do so for prostate cancers and brain tumors. These results demonstrate that the transcriptional network-inferred PTEN-controlled TFAs are generally more reliable than expression-based gene sets in representing PTEN functional status.

Specific sets of PTEN-controlled TFAs preferentially contribute to different tumor development

Given that the PTEN-controlled TFA signatures are associated with PTEN status in prostate, breast and brain tumors, we next asked if a particular subset of the transcription factors play more important role in each individual tumor type. To this end, we first compared each TFA between PTEN positive and negative samples, identified by both IHC/CN and TFA-based analysis. Figure 6A shows the \log_{10} transformed p-value of the t-test of such comparisons in each tumor type. The first six TFAs, i.e., HLF, ELK1, JUN, SMAD1, STAT6 and c-MYC, are significantly ($p < 0.05$) altered in the PTEN negative group in all three cancers. STAT6 TFA is decreased while the others TFA are increased in the PTEN negative group. The degree of overlap of the tumor type-specific PTEN-controlled TFAs is summarized by a Venn diagram in Figure 6B.

We further investigated the possible interactions among the TFAs by examining pair wise correlation coefficients of inferred TFAs across patient tumors in each tissue type. The absolute correlation coefficients between the pairs are illustrated in Figure 6C–E for human prostate, breast and brain tumors, respectively. In general, the TFAs that more significantly track with PTEN status are highly correlated with each other, and assemble together into clusters that may reflect common upstream signaling-based activation mechanisms. Notably, in each tumor type, more than one TFA clusters are formed, suggesting that PTEN regulates TFAs through more than a single signaling pathway. The overlapping and specific TFA signatures in different types of human cancers provide a transcription factor-based guide to the mechanisms of cancer development caused by PTEN loss, and offer TFA-based rationales for designing new therapeutic regimen for treating PTEN null cancers and also monitoring PI3K pathway targeted treatment responses.

Discussion

In this study we used NCA and its complementary trimming algorithm to reveal 20 TFs that immediately respond to the expression of PTEN in a PTEN inducible system. We found that the PTEN immediate responsive gene-based TFA signatures are more accurate and sensitive than either cancer-based TFA or gene expression-based analyses in predicting PTEN functional status in human cancers. These TFA-based signatures, therefore, provide readout of transcription factor activity even if their mRNA levels do not change, and help to overcome the complexity of

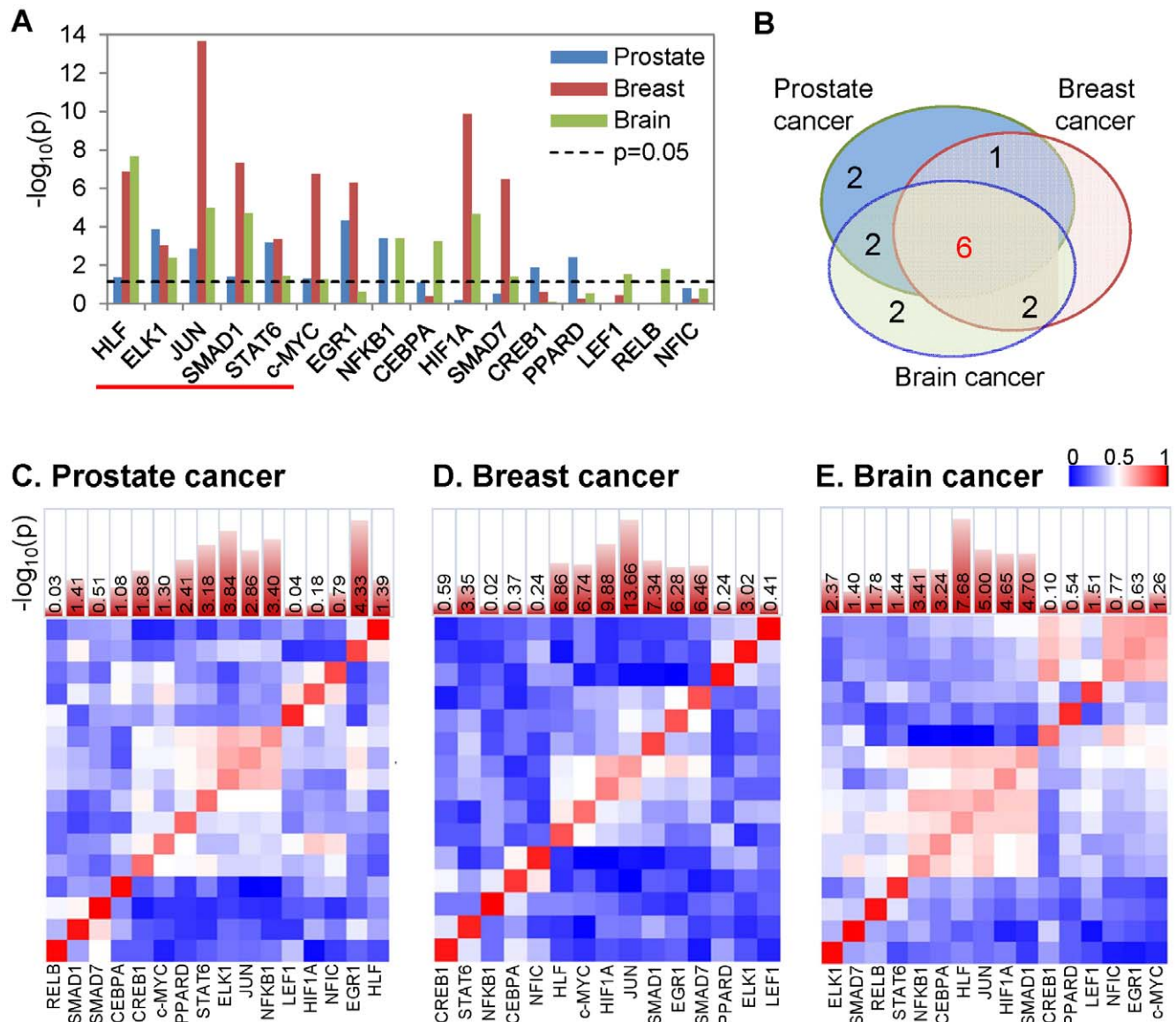


Figure 6. Subsets of PTEN-controlled TFs preferentially function in specific types of tumors. (A) t-test p-values comparing TFs of the subgroups based on PTEN status and clustering results as shown in Figure 5 in three tumor types. In the t-tests performed on of prostate and breast cancers, PTEN positive samples in group 3 were used as the PTEN positive functional status, the PTEN negative samples in group 1 as the PTEN negative functional status. Similarly, in brain tumor PTEN IHC positive samples in group 2 and PTEN IHC negative samples in group 1 were selected for representing PTEN positive and negative functional status respectively. The red line highlighted the 6 TFs significantly ($p < 0.05$) altered between tumor subgroups in three tumor types. (B) Venn diagram summarizing the overlap of the TFs that contribute to the discrimination of tumor subgroups with different PTEN status in different tumor types. (C–E) Heatmap of the absolute Pearson correlation coefficients between NCA-inferred TF activity profiles across the tumor samples from prostate (C), breast (D) and brain (E) cancers, indicating groups of co-active transcription factors may function together.

doi:10.1371/journal.pone.0031053.g006

multifactorial post-transcriptional PTEN signaling pathway regulations. Since mRNA profiles are currently measureable in clinical settings, our TFA-based signatures provide new rationales for stratifying patients according to their PTEN functional status and for monitoring treatment outcome in PI3K-targeted therapies.

Our study testifies to the power of combining traditional genetic and biochemical approaches with mathematic algorithms in deciphering complicated transcription regulatory networks. NCA complements other classical bioinformatics methods, such as Principal Component Analysis (PCA) and Independent Component Analysis (ICA). In contrast to PCA and ICA, NCA utilizes biochemical constraints, i.e., the relationship between transcription

factors and their regulated genes, rather than statistical or mathematical constraints in data deconvolution. This means if target genes of a certain TF concordantly altered their expressions, even though at the subtle levels upon stimulation, its NCA-derived TFA will show significant changes. Besides, NCA also detangles effects of multiple TFs regulating a same gene. TFA profiles are more robust and reliable in representing the real activities than the expression of a TF specific target gene which may not be expressed in all tissues. This explains why TFA-based signatures are more reliable than gene-based signatures in predicting PTEN status in different tumor types. NCA has been used to reveal biological relevant network structure and regulatory dynamics in bacteria [17,39,40,41,42], *Saccharomyces*

cerevisiae [41,43] and mouse [44]. In our study, the PTEN-controlled TFA signatures deduced by our NCA analysis have been validated experimentally and bioinformatically across in vitro cell lines, in vivo animal models and in patient samples.

A shortcoming of NCA is that it depends on the information of TF and target gene relationship. For instance, although FOXO activity is known to be regulated by PTEN controlled PI3K/AKT pathway, FOXO TFA cannot be derived in PTEN inducible system because its target gene expression values are not available in the database we used. Nevertheless, the results obtained from our analyses are quite robust.

Although PTEN is not a TF, it can regulate TFAs through either phosphatase-dependent or -independent mechanisms. In the prostate cancer mouse models, the majority of TFs perturbed in the *Pten* null mouse exhibit concordant alterations in their activities when the PTEN downstream AKT/mTOR pathway is manipulated genetically or pharmaceutically by the mTOR inhibitor rapamycin. This result implies that PTEN controls TFAs through its phosphatase activity by regulating the PI3K/AKT/mTOR pathway, which is known for regulating activities of several TFs including NF- κ B [23], p53 [10], FOXO [9] and CREB [45]. These TFs may also serve as co-activators or repressors for other TFs. Interestingly, we found c-MYC level and activity is directly regulated by PTEN expression and a significant overlap between *hi-c-Myc* and *Pten* null or *mAKT1* prostate cancer models in their associated prostate cancer-associated TFAs. It is worthy to note that c-MYC target genes that are perturbed by *PTEN* expression involve the regulation of cell growth, cell metabolism, and protein synthesis [46,47,48,49], suggesting that the c-MYC-regulated target genes may potentially play important roles in the development of PTEN-deficient cancers. PTEN can also function independent of its phosphatase activity to regulate cell migration [50], p53 [10] and APC-CDH2 [51]. It is conceivable that PTEN regulates a subset of TFAs, such as EGR1, LEF1, HLF, and STAT6 (Figure 3), through its phosphatase-independent functional domains [6]. Whether PTEN needs to be located in the nuclear to perform such a function requires further investigation.

Our study reveals common and cancer tissue type-specific regulation of TFAs by the PTEN tumor suppressor. The six common PTEN-controlled TFAs including c-MYC most likely play an essential role in tumor development caused by PTEN loss and their activity may serve as surrogate markers for determining PTEN functional status and measuring response to targeted therapy. Other tissue-type-specific regulated TFAs may help us understand PTEN's tissue-specific function. The PTEN-controlled TFAs deduced by NCA, therefore, will aid in stratifying cancer patients according to PTEN functional status and in deciphering the complicated transcription regulatory networks controlled by the PTEN tumor suppressor. Although targeting transcription factors with small molecules remains challenging, recent works by Bradner and colleagues on selective inhibitions of BET bromodomains [52] and NOTCH transcription factor complex [53] provide promising direction of this approach. Since efficient targeting the intermediate effectors of the PTEN controlled signaling pathway is difficult because of the feedback loops and cross-talks among intracellular signaling pathways, our study may guide the future efforts in targeting PTEN deficient cancers through disrupting its regulated transcriptional architectures.

Materials and Methods

Cell culture and transfection

PTEN-inducible mouse *Pten*^{ΔloxP/ΔloxP} MEF cells [21] or PC3 [6,54] cells were cultured in DMEM or RPMI medium,

respectively, supplemented with 10% tetracycline-free fetal calf serum (Invitrogen), 100 U/ml penicillin and streptomycin (Gibco).

Real-time PCR

Total RNAs were extracted using RNeasy Mini kit (Qiagen). RNAs were reverse-transcribed by oligo(dT) primer using Superscript RT-PCR kit (Invitrogen), according to the manufacturer instructions. PCR reaction was performed under the following conditions: 94°C for 3 min; 94°C 30 Sec; 58°C for 30Sec; 72°C for 30 Sec for 40 cycles; and 72°C for 10 min, using iQ SYBER Green Supermix Kit from Bio-Rad. Results were analyzed by the relative quantification method and expressed as relative RNA levels (Δ CT, difference of cycling threshold). Δ CT values represent CT [gene]-CT [GAPDH], thus higher values indicate relatively lower expression levels. Primer sequences used for real-time PCR were retrieved from PrimerBank website.

Chromatin immunoprecipitation (ChIP) assay

Chromatin immunoprecipitations were modified from the EZ-ChIP (Upstate) protocol using antibodies: anti-c-Myc (A14, Santa Cruz) anti-LEF1 (C-19, Santa Cruz). The percentage of the bound DNA was quantified against the original DNA input using real time PCR analysis (Biorad). Primer sequences used for ChIP are as follows:

BCAT-5': AATCCGCTAGGTCGCGAGT; BCAT-3': AGCA-AGACCTGGGGCAGT

CDK4-5': TTACACTCTTCGCCCTCCTC; CDK4-3': ATG-TGACCAGCTGCCAAAG

EIF4E-5': CAGGGCCAAACGGACATA; EIF4E-3': CAATA-CTCACCGTTTCGACA

SHMNT1-5': GCAGAGTGCACCTTCCTGA;

SHMNT1-3': GTGCCACCAGTCCCAGAC

WISP1-5': GGGATAGCAAGCATCCAGAG;

WISP1-3': CCTTCATGACACGTGAAAGC

DNA microarray data preprocessing

All the array datasets were downloaded from public domains, and were MIAME compliant. Mouse and MEF expression data was available through NCBI's Gene Expression Omnibus (GEO) with accession IDs GSE29010 and GSE1413, and normalized by RMA method. Human expression data sets were downloaded from GEO and other public domains (see Text S1). If a gene has multiple probesets representing it, its expression was evaluated as the average of its probesets.

Transcription factor activity (TFA) analysis

NCA is built based on log-linear model in which gene expression ratios are log-linearly proportional to activity ratios of their regulators. In the NCA pre-processing steps, expression data sets from single channel Affymetrix arrays were set in log ratios comparing the conditions of interest (e.g. *Pten* null, *hi-Myc*, tumors) to the references (e.g. WT, normal). Biological repeat arrays were averaged first before calculating the log ratios to filter out extreme value of log-ratio.

We used the network structure information provided by Transcriptional Regulatory Element Database (TRED) from Cold Spring Harbor Laboratory [55], in which the connectivity information is based on experimental validation and motif searching. NCA and trimming algorithm [16] were used to reconstruct the transcriptional network for each data set. In the study, we only used the experimental-based TF-gene relationships to minimize the false positive connection defined by motif searching. The statistical significance of TFAs in murine datasets

was justified based on random sampling network expression [16]. In brief, we first generate $n \sim 200$ random networks whose gene expression data is random sampled from whole genome. Such random networks are then analyzed by NCA using the same network structure as the interested one. The collection of TFAs obtained from analyzing random networks form the null distributions. For each original TFA in individual experiments, the TFA modified z-score was calculated based on the median and median of absolute deviation to determine how significantly the TFA is perturbed under the experimental conditions. The median and median of absolute deviation, instead of mean and standard deviation, are used to avoid the effect of outliers.

Clustering analysis

Cluster 3.0 was used for the unsupervised hierarchical clustering analysis using TFAs/gene expression. The similarity between samples was represented by the cosine (or un-centered correlation) metric. Complete linkage was used to clusters samples. In the heatmap of prostate data the TFAs are colored code based on their relative values to the respective averages of normal samples to illustrate the direction of TFA variation to normal prostate tissue.

Pair wise correlation coefficient analysis

In each human cancer dataset, Pearson correlation coefficient between each pair of TFAs was calculated. The unsupervised hierarchical clustering analysis was then used to rearrange the order of TFAs in the matrix of the absolute correlation coefficients.

Western blot analysis

Whole-cell extraction was described detail in [21]. Cell lysates were subjected to 10% sodium dodecyl sulfate-polyacrylamide gel electrophoresis, transferred onto nitrocellulose (Bio-Rad), and followed by Western blot analysis using PTEN (9552; Cell Signaling), c-MYC (Santa Cruz), STAT6 (Santa Cruz), p-STAT6 (Abcam), JUN and p-JUN (Cell Signaling) antibodies. Quantification was performed with BioRad Image Lab software.

Supporting Information

Figure S1 Validation of PTEN-inducible systems. (A) Restoration of *PTEN* expression suppressing the expression of the p90 isoform, but not p76 isoform of MDM2 in *PTEN* inducible PC3 cells. (B) *PTEN* re-expression does not change the c-MYC, STAT6 and c-JUN total protein levels but does alter the ratio of phosphor-c-JUN to total c-JUN. Numbers indicate the relative ratio of phosphorylated to total protein, or the levels of c-Myc protein, with the PTEN null state defined as unity. (TIFF)

References

- Di Cristofano A, Pandolfi PP (2000) The multiple roles of PTEN in tumor suppression. *Cell* 100: 387–390.
- Orloff MS, Eng C (2008) Genetic and phenotypic heterogeneity in the PTEN hamartoma tumour syndrome. *Oncogene* 27: 5387–5397.
- Nagata Y, Lan KH, Zhou X, Tan M, Esteva FJ, et al. (2004) PTEN activation contributes to tumor inhibition by trastuzumab, and loss of PTEN predicts trastuzumab resistance in patients. *Cancer Cell* 6: 117–127.
- She QB, Solit DB, Ye Q, O'Reilly KE, Lobo J, et al. (2005) The BAD protein integrates survival signaling by EGFR/MAPK and PI3K/Akt kinase pathways in PTEN-deficient tumor cells. *Cancer Cell* 8: 287–297.
- Salmena L, Carracedo A, Pandolfi PP (2008) Tenets of PTEN tumor suppression. *Cell* 133: 403–414.
- Mossessian S, Avliyakov NK, Mulholland DJ, Boontheung P, Loo JA, et al. (2009) Analysis of PTEN complex assembly and identification of heterogeneous nuclear ribonucleoprotein C as a component of the PTEN-associated complex. *J Biol Chem* 284: 30159–30166.

Figure S2 Heatmap of TFAs changes deduced from gene expression profiles in PTEN inducible MEFs and prostate cancer mouse models. Heatmap showing PTEN-controlled TFAs that are significantly altered in PTEN-inducible MEF tissue culture cells; and a set of prostate cancer-related TFAs that are significantly altered during tumorigenesis in murine prostate cancer models, but not by re-expression of PTEN in the PTEN-inducible MEF system (Rapa: Rapamycin treatment). (TIF)

Figure S3 The PTEN-control TFA-based unsupervised clustering analysis. Unsupervised clustering analysis, based on PTEN-controlled TFAs, was used to classify human tumor samples. (A) the first and (B) the second (NKI) breast cancer data sets and in (C) brain cancer dataset. In the first breast tumor data set (A), PTEN-controlled TFA-based unsupervised clustering yields a clustering pattern of tumor PTEN negative status (Group 1). As for the second breast cancer data set the dendrogram also illustrates the association of PTEN-negative Group 1 with poorly differentiated, ER-negative and basal-like phenotype. (TIF)

Figure S4 NCA-inferred TFAs significantly altered in human breast cancer based on PTEN IHC. Log₁₀-transformed t-test p values for each TFA between samples of different IHC-based PTEN status. The graph shows the 45 TFs with the highest log₁₀-transformed p-values. The p-values >0.1 of the other 25 TFs are not shown. The dashed line ($p = 1e-4$) indicates the threshold value for selecting the TFA-based PTEN-IHC-derived signatures used in the analysis in Figure 5 (gold). (TIF)

Table S1 List of PTEN immediately controlled genes in MEFs. (XLS)

Text S1 Supporting Information. (DOC)

Acknowledgments

We appreciate the helpful comments and suggestions from colleagues in our laboratories.

Author Contributions

Conceived and designed the experiments: LMT C-JC JCL TGG HW. Performed the experiments: C-JC SW JD. Analyzed the data: LMT C-JC PSM TGG HW. Contributed reagents/materials/analysis tools: SP PSM. Wrote the paper: LMT C-JC TGG HW.

13. Yuan TL, Cantley LC (2008) PI3K pathway alterations in cancer: variations on a theme. *Oncogene* 27: 5497–5510.
14. Chandarlapaty S, Sawai A, Scaltriti M, Rodrik-Outmezguine V, Grbovic-Huezo O, et al. (2011) AKT inhibition relieves feedback suppression of receptor tyrosine kinase expression and activity. *Cancer Cell* 19: 58–71.
15. Liao JC, Boscolo R, Yang YL, Tran LM, Sabatti C, et al. (2003) Network component analysis: reconstruction of regulatory signals in biological systems. *Proc Natl Acad Sci U S A* 100: 15522–15527.
16. Tran LM, Hyduke DR, Liao JC (2010) Trimming of mammalian transcriptional networks using network component analysis. *BMC Bioinformatics* 11: 511.
17. Zhang Y, Hatch KA, Bacon J, Wernisch L (2010) An integrated machine learning approach for predicting DosR-regulated genes in *Mycobacterium tuberculosis*. *BMC Syst Biol* 4: 37.
18. Harbison CT, Gordon DB, Lee TI, Rinaldi NJ, Macisaac KD, et al. (2004) Transcriptional regulatory code of a eukaryotic genome. *Nature* 431: 99–104.
19. Orian A, Abed M, Kenyagin-Karsenti D, Boico O (2009) DamID: a methylation-based chromatin profiling approach. *Methods Mol Biol* 567: 155–169.
20. Jiang C, Xuan Z, Zhao F, Zhang MQ (2007) TRED: a transcriptional regulatory element database, new entries and other development. *Nucleic Acids Res* 35: D137–140.
21. Chang CJ, Freeman DJ, Wu H (2004) PTEN regulates Mdm2 expression through the P1 promoter. *J Biol Chem* 279: 29841–29848.
22. Mulholland DJ, Tran LM, Li Y, Cai H, Morim A, et al. (2011) Cell autonomous role of PTEN in regulating castration-resistant prostate cancer growth. *Cancer Cell* 19: 792–804.
23. Madrid LV, Mayo MW, Reuther JY, Baldwin AS, Jr. (2001) Akt stimulates the transactivation potential of the RelA/p65 Subunit of NF-kappa B through utilization of the Ikappa B kinase and activation of the mitogen-activated protein kinase p38. *J Biol Chem* 276: 18934–18940.
24. Majumder PK, Febbo PG, Bikoff R, Berger R, Xue Q, et al. (2004) mTOR inhibition reverses Akt-dependent prostate intraepithelial neoplasia through regulation of apoptotic and HIF-1-dependent pathways. *Nat Med* 10: 594–601.
25. Vivanco I, Rohle D, Versele M, Iwanami A, Kuga D, et al. (2010) The phosphatase and tensin homolog regulates epidermal growth factor receptor (EGFR) inhibitor response by targeting EGFR for degradation. *Proc Natl Acad Sci U S A* 107: 6459–6464.
26. Vivanco I, Palaskas N, Tran C, Finn SP, Getz G, et al. (2007) Identification of the JNK signaling pathway as a functional target of the tumor suppressor PTEN. *Cancer Cell* 11: 555–569.
27. Taylor BS, Schultz N, Hieronymus H, Gopalan A, Xiao Y, et al. (2010) Integrative genomic profiling of human prostate cancer. *Cancer Cell* 18: 11–22.
28. Wang S, Gao J, Lei Q, Rozengurt N, Pritchard C, et al. (2003) Prostate-specific deletion of the murine Pten tumor suppressor gene leads to metastatic prostate cancer. *Cancer Cell* 4: 209–221.
29. Wang S, Garcia AJ, Wu M, Lawson DA, Witte ON, et al. (2006) Pten deletion leads to the expansion of a prostatic stem/progenitor cell subpopulation and tumor initiation. *Proc Natl Acad Sci U S A* 103: 1480–1485.
30. Ellwood-Yen K, Graeber TG, Wongvipat J, Iruela-Arispe ML, Zhang J, et al. (2003) Myc-driven murine prostate cancer shares molecular features with human prostate tumors. *Cancer Cell* 4: 223–238.
31. The Cancer Genome Atlas Research Network (2008) Comprehensive genomic characterization defines human glioblastoma genes and core pathways. *Nature* 455: 1061–1068.
32. Saal LH, Johansson P, Holm K, Gruvberger-Saal SK, She QB, et al. (2007) Poor prognosis in carcinoma is associated with a gene expression signature of aberrant PTEN tumor suppressor pathway activity. *Proc Natl Acad Sci U S A* 104: 7564–7569.
33. Freije WA, Castro-Vargas FE, Fang Z, Horvath S, Cloughesy T, et al. (2004) Gene expression profiling of gliomas strongly predicts survival. *Cancer Res* 64: 6503–6510.
34. Lapointe J, Li C, Higgins JP, van de Rijn M, Bair E, et al. (2004) Gene expression profiling identifies clinically relevant subtypes of prostate cancer. *Proc Natl Acad Sci U S A* 101: 811–816.
35. Lapointe J, Li C, Giacomini CP, Salari K, Huang S, et al. (2007) Genomic profiling reveals alternative genetic pathways of prostate tumorigenesis. *Cancer Res* 67: 8504–8510.
36. van de Vijver MJ, He YD, van't Veer LJ, Dai H, Hart AA, et al. (2002) A gene-expression signature as a predictor of survival in breast cancer. *N Engl J Med* 347: 1999–2009.
37. Sorlie T, Perou CM, Tibshirani R, Aas T, Geisler S, et al. (2001) Gene expression patterns of breast carcinomas distinguish tumor subclasses with clinical implications. *Proc Natl Acad Sci U S A* 98: 10869–10874.
38. Palaskas N, Larson SM, Schultz N, Komisopoulou E, Wong J, et al. (2011) 18F-fluorodeoxy-glucose Positron Emission Tomography (18FDG-PET) Marks Basal-Like Human Breast Cancer with MYC Overexpression. *Cancer Research* 71.
39. Kao KC, Tran LM, Liao JC (2005) A global regulatory role of gluconeogenic genes in *Escherichia coli* revealed by transcriptome network analysis. *J Biol Chem* 280: 36079–36087.
40. Kao KC, Yang YL, Boscolo R, Sabatti C, Roychowdhury V, et al. (2004) Transcriptome-based determination of multiple transcription regulator activities in *Escherichia coli* by using network component analysis. *Proc Natl Acad Sci U S A* 101: 641–646.
41. Yang YL, Suen J, Brynildsen MP, Galbraith SJ, Liao JC (2005) Inferring yeast cell cycle regulators and interactions using transcription factor activities. *BMC Genomics* 6: 90.
42. Hyduke DR, Jarboe LR, Tran LM, Chou KJ, Liao JC (2007) Integrated network analysis identifies nitric oxide response networks and dihydroxyacid dehydratase as a crucial target in *Escherichia coli*. *Proc Natl Acad Sci U S A* 104: 8484–8489.
43. Tan K, Feizi H, Luo C, Fan SH, Ravasi T, et al. (2008) A systems approach to delineate functions of paralogous transcription factors: role of the Yap family in the DNA damage response. *Proc Natl Acad Sci U S A* 105: 2934–2939.
44. Rahib L, Sriram G, Harada MK, Liao JC, Dipple KM (2009) Transcriptomic and network component analysis of glycerol kinase in skeletal muscle using a mouse model of glycerol kinase deficiency. *Mol Genet Metab* 96: 106–112.
45. Huang H, Cheville JC, Pan Y, Roche PC, Schmidt LJ, et al. (2001) PTEN induces chemosensitivity in PTEN-mutated prostate cancer cells by suppression of Bcl-2 expression. *J Biol Chem* 276: 38830–38836.
46. Hermeking H, Rago C, Schuhmacher M, Li Q, Barrett JF, et al. (2000) Identification of CDK4 as a target of c-MYC. *Proc Natl Acad Sci U S A* 97: 2229–2234.
47. Meyer N, Penn LZ (2008) Reflecting on 25 years with MYC. *Nat Rev Cancer* 8: 976–990.
48. Nikiforov MA, Chandriani S, O'Connell B, Petrenko O, Kutenko I, et al. (2002) A functional screen for Myc-responsive genes reveals serine hydroxymethyltransferase, a major source of the one-carbon unit for cell metabolism. *Mol Cell Biol* 22: 5793–5800.
49. Rosenwald IB, Rhoads DB, Callanan LD, Isselbacher KJ, Schmidt EV (1993) Increased expression of eukaryotic translation initiation factors eIF-4E and eIF-2 alpha in response to growth induction by c-myc. *Proc Natl Acad Sci U S A* 90: 6175–6178.
50. Raftopoulos M, Etienne-Manneville S, Self A, Nicholls S, Hall A (2004) Regulation of cell migration by the C2 domain of the tumor suppressor PTEN. *Science* 303: 1179–1181.
51. Song MS, Carracedo A, Salmena L, Song SJ, Egia A, et al. (2011) Nuclear PTEN regulates the APC-CDH1 tumor-suppressive complex in a phosphatase-independent manner. *Cell* 144: 187–199.
52. Filippakopoulos P, Qi J, Picaud S, Shen Y, Smith WB, et al. (2010) Selective inhibition of BET bromodomains. *Nature* 468: 1067–1073.
53. Moellering RE, Cornejo M, Davis TN, Del Bianco C, Aster JC, et al. (2009) Direct inhibition of the NOTCH transcription factor complex. *Nature* 462: 182–188.
54. Wang B, Chen J, Santiago FS, Janes M, Kavurma MM, et al. (2010) Phosphorylation and acetylation of histone H3 and autoregulation by early growth response 1 mediate interleukin 1beta induction of early growth response 1 transcription. *Arterioscler Thromb Vasc Biol* 30: 536–545.
55. Zhao F, Xuan Z, Liu L, Zhang MQ (2005) TRED: a Transcriptional Regulatory Element Database and a platform for in silico gene regulation studies. *Nucleic Acids Res* 33: D103–107.